

Focusing capillar and porous X-ray optics

© V.V. Lider

Shubnikov Institute of Crystallography „Crystallography and Photonics“, Russian Academy of Sciences, Moscow, Russia

e-mail: vallider@yandex.ru

Received on May 29, 2021

Revised on May 29, 2021

Accepted on July 21, 2021

The paper discusses the principles and capabilities of X-ray focusing capillar and porous optics. Special attention is paid to polycapillar optics, confocal technique of X-ray fluorescence analysis, as well as wide-angle „lobster eye“ optics.

Keywords: X-rays, focusing, capillar, porous optics, „lobster eye“ optics.

DOI: 10.21883/EOS.2022.14.54002.19-21

1. Introduction

Over the past three decades, a large number of publications have appeared devoted to the non-destructive study of condensed mediums using X-ray microbeam [1].

The condensing optics used to form the X-ray microbeam is traditionally a large-diameter Fresnel-zone plate with tens of thousands of zones [2]. The Fresnel-zone plate has a limited bandwidth, which can be useful in applications where it is necessary to isolate a certain spectral line from a laboratory X-ray source, but is a disadvantage when synchrotron radiation (SR) is used. Besides, the Fresnel-zone plates are fragile and have low efficiency.

Recently, alternative types of condenser (concentrator) based on hollow glass capillaries have been developed. Focusing capillaries use the effect of total external reflection (TER) of X-rays from the inner walls of channels having the shape of an ellipsoid or a paraboloid of revolution. These optical elements are achromatic and therefore do not act as monochromators as in the case of Fresnel-zone plates. Such capillaries provide uniform illumination of the sample with a hollow cone of X-rays and the formation of a focal spot with size of $\sim 1 \mu\text{m}$ [3].

Capillaries have a number of advantages over Fresnel-zone plates used as a condenser [4]: 1) they are more accessible, 2) allow energy tuning using a monochromator without the need to move the condenser when the X-ray energy changes, 3) their efficiency is by 3–15 times higher than the efficiency of zone plates in the absence of undesirable high diffraction orders, 4) they are more reliable, more durable, 5) are resistant to thermal load or mechanical damages, 6) do not require a diaphragm installed near the focus to form the necessary bandwidth and, thus, do not limit the size of the sample holder and the ability to control it.

Capillaries bent in a special way make it possible to create multiple reflection systems capable to control the direction of X-ray propagation. By bringing together a large number of capillaries, curved with different radii of curvature, and

arranging them in such a way that they direct radiation to a single point, an effective X-ray lens can be created.

However, ellipsoidal surfaces are characterized by serious off-axis aberrations. Therefore, capillar optics is not imaging. But for the condenser, the defocusing of off-axis radiation does not matter as long as the source is small enough, and the illumination distribution at the corners is the same over the area of the sample.

The situation changes when it is necessary to create efficient X-ray imaging optics, used, for example, in X-ray orbital telescopes. In order to reduce aberrations, they usually use composite grazing-incidence mirror systems, known as Voltaire I systems [5,6], in which radiation is successively reflected from two aspherical surfaces. To increase the effective collection area of the telescope, several coaxial and confocal mirrors are used, tightly nested in each other. However, density increasing of the mirrors packing leads to increased weight of the optics, which makes it difficult to put the equipment into a near-Earth orbit. Porous optics makes it possible to significantly reduce the telescope weight while maintaining the density of reflecting surfaces, and, hence, its efficiency [7].

One of the directions in the development of focusing porous optics is based on the use of silicon wafers with stiffeners. The wafers are stacked on top of each other, forming channels of a square profile of submillimeter size. This design can successfully replace densely packed mirrors in Voltaire I optics, providing unexampled light weight and rigidity of the structure.

Another direction in the development of focusing porous optics is based on the use of a spherically curved glass microporous plate, and the use of square profile channels for X-ray focusing can become the equivalent of the so-called optics of „lobster eye“ [8].

2. Focusing capillar X-ray optics

At present X-ray capillar optics is an independent direction in optics [9]. Capillar X-ray optical systems

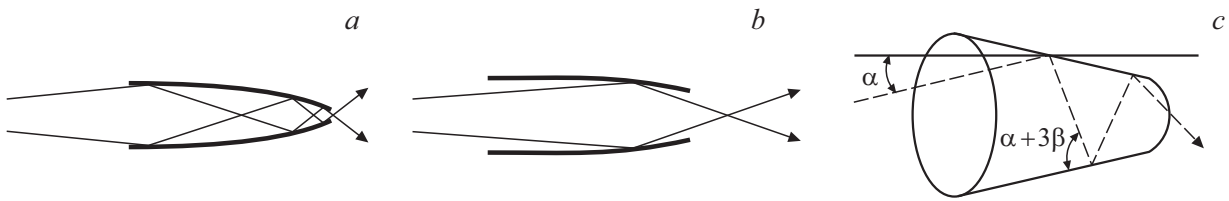


Figure 1. The path of rays in a monocapillary of multiple (a), single (b) reflection and in a conical capillary [17] (c) (see text).

make it possible to effectively form X-ray beams of the required configuration in a wide energy range; they are also simple in design and manufacturable. A very important property of capillar optical elements is the fundamental possibility of obtaining a greater luminosity compared to other optical focusing elements in the X-ray range, which makes it possible to use capillar systems as effective X-ray concentrators. Unlike conventional methods of X-radiation focusing, the capillar optics makes it possible to actually control X-ray beams [10–13].

The problem of cutting off the hard part of electromagnetic radiation is a problem in radiation physics. The hard part of the X-ray spectrum can be filtered using capillar systems. The filtering mechanism is related to the fact that X-rays propagate inside the channels, reflecting from their walls, provided that the grazing angle θ ($\theta \leq \theta_c$) is small. The value of TER critical angle θ_c is given by the approximate formula:

$$\theta_c(\text{mrad}) \approx 2.34\lambda(Z\rho/A)^{1/2}, \quad (1)$$

where ρ (g/cm^3) is density of the material, Z and A are its atomic number and weight, respectively, λ (\AA) is X-ray wavelength.

Since the angle θ_c is proportional to the X-ray wavelength, then, by selecting a certain geometry of the optical system, it is possible to achieve that the channeling condition (propagation inside the channel) is violated for the short-wavelength part of the radiation spectrum, and the throughput of the system is reduced. On the other hand, in the region of long wavelengths, the throughput of the system also decreases due to the increased radiation absorption in this range. Thus, each specific capillar system has a natural working bandwidth.

As studies have shown [14–16], the quality of the inner surface of glass capillaries is quite suitable for use in X-ray optics. This means that such capillaries can serve as effective waveguides for X-rays, i.e. to transport the radiation entering them in a rather wide spectrum with losses that are significant only for a very large number of reflections, since losses per one reflection can be minimized with an appropriate selection of the capillary material and the quality of its inner surface. For typical grazing angles $\theta \sim \theta_c/2$, the roughness height, as a rule, shall not exceed 10–20 \AA [9].

Obviously, X-ray capillar optics can be used in all areas where it is necessary to increase the X-ray flux density, and where control over their propagation is necessary.

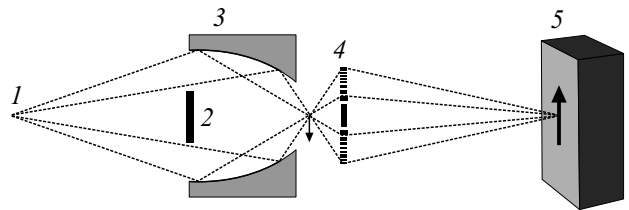


Figure 2. Scheme of a total field of view X-ray microscope with an ellipsoidal capillary as condenser: 1 — radiation source, 2 — plug, 3 — capillary, 4 — lens Fresnel-zone plate, 5 — detector [3].

2.1. Monocapillary X-ray optics

Figure 1, a, b shows the difference between two types of monocapillar optics: multiple and single reflection. In the first case, the X-rays after several successive reflections form a focal spot, the size of which is determined by the size of the outlet and the properties of the radiation source. The throughput of the capillary depends on the number of reflections, the quality of the optics, etc., and usually ranges from 10 to 80%. Disadvantage is that the focus is in close proximity to the capillary output: typically, to obtain a small size of the focus, the sample must be placed at a distance of 10–100 μm for a micron size of the focal spot.

In order to be able to obtain a focus distance from the outlet equal to millimeters or centimeters, a single reflection monocapillary can be used (Fig. 1, b). It shows almost 100% throughput, since the single reflection is very effective in TER conditions [18].

Note that due to the significant beam divergence at the capillary output, the focal spot size d_f will always be larger than the capillary output size d_{out} due to the nonzero focal length f , i.e. from the distance from the capillary end to the sample [14,19]:

$$d_f \approx d_{\text{out}} + 2f\theta_c. \quad (2)$$

Monocapillaries based on single reflection usually have elliptical or parabolic shape [20]. Using the elliptical capillary, a point source can be focused if the source is located at one of the foci of the ellipse. The focal spot will then appear at the second focus. A parabolic capillary can focus a parallel beam or transform the X-ray beam diverging from the point source into a parallel beam. The size of the focal spot will be determined not only by the manufacturing accuracy of the optical element, but also by the properties

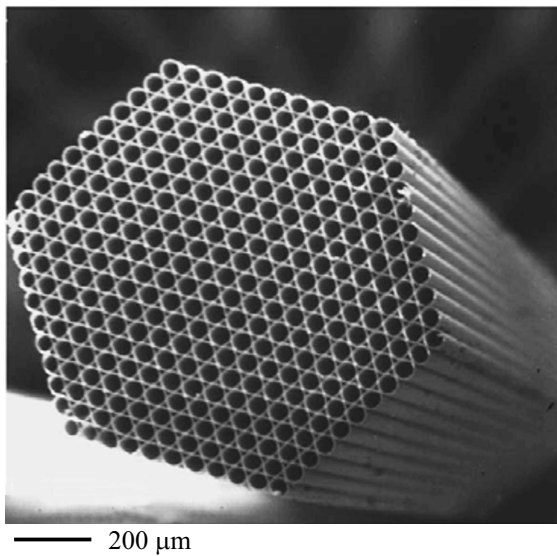


Figure 3. Micrograph of cross section of polycapillar lens obtained using scanning electron microscope. Channel diameter $\sim 50 \mu\text{m}$ [55].

of the radiation source [21]. In this paper [22] the X-ray beam with an energy of 30 keV was focused by means of elliptical single reflection capillary into the focal spot $15 \mu\text{m}$ in size.

One of the ways to obtain X-ray beams with submicron sizes is the use of a conical capillary narrowing according to the law of ellipse or parabola [17,23–27]. The authors of the paper [25] obtained a spatial resolution of 50 nm at $E = 5\text{--}8 \text{ keV}$. This is the highest resolution obtained with X-ray monocabillary optics.

In conical capillary (Fig. 1,c) X-rays experience TER from the smooth inner surface of the capillary at angles of incidence α smaller than the critical angle θ_c . The first reflection occurs at angle $\alpha + \beta$, where β is the half angle of opening of the capillary cone. The second reflection occurs at the angle $\alpha + 3\beta$, and the n -th — at the angle $\alpha + (2n - 1)\beta$. At the angle of incidence greater than the critical one, the X-rays do not participate in the focusing process. Thus, the number of effective reflections is determined by the inequation: $n < (\theta_c - \alpha + \beta)/2\beta$ [17,19].

Monocabillary optics is used as X-ray concentrators with various radiation sources: SR [3,28–31], X-ray tube [32,33], laser-plasma sources [34,35].

Single reflection concentrator-capillaries support a wide range of applications, including X-ray fluorescence [36–40] and tomography [41], X-ray microscopy [3,42–44] (Fig. 2), small-angle scattering of X-rays [45], diffraction methods [28,45–48].

2.2. Polycapillar X-ray optics

The simplest element of capillar optics is a straight cylindrical capillary, which is a hollow glass tube of a cylindrical shape. With the help of such capillary, a change

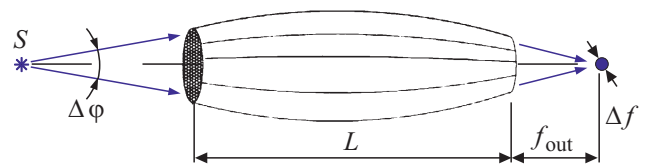


Figure 4. X-rays focusing scheme with a polycapillar lens (S — radiation source, $\Delta\varphi$ — receiving aperture, L — lens length, f_{out} — focal length, Δf — focal spot size).

in the direction of radiation propagation can be carried out, since the X-rays can be kept in a hollow, slightly curved capillary. When bending the capillary, consider that not all rays entering the channel will satisfy the condition $\theta < \theta_c$. Assuming that the inner radius of the capillary r_0 is small compared to the radius of the capillary bend R ($r_0/R \ll 1$) and taking into account the small TER critical angle for X-rays, the condition for effective radiation capture in the mode of radiation transportation by the capillary is written as

$$(R/r_0)(\theta_c/2)^2 \geq 1. \quad (3)$$

Thus, the maximum angle of rotation of the X-ray beam Ψ_{max} by the capillary with length L is determined by the expression

$$\Psi_{\text{max}} = (L/r_0)(\theta_c/2)^2. \quad (4)$$

In the literature the possibility of using capillaries as X-ray beam control elements was described and substantiated quite a long time ago [14,49]. It was shown that bent capillary is fundamentally capable of turning a beam of hard X-ray radiation through angles up to 10° with efficiency up to 10% [50].

By bringing together a large number of capillaries, curved with different radii of curvature, and arranging them in such a way that they direct radiation to a single point, the X-ray lens can be created. Such system is polycapillar lens (Kumakhov's optics) consisting of many curved channels [51–56]. For each channel, as for mirror, the radiation capture angle does not exceed double critical angle, but there are many channels, and the actual capture angle of lens can reach several degrees, exceeding the critical angle by tens and hundreds of times.

The condition $\theta < \theta_c$ requires the use of small channels, usually from 2 to $50 \mu\text{m}$ (Fig. 3). Due to the mechanical limitations of thin-wall tubes of this size production, the optics are made using a repeated folding and drawing process of glass fiber optics [57].

The polycapillar system, designed in a certain way, allows not only to efficiently transport radiation, but also to increase the radiation density by focusing it into a spot of micron size Δf . Therefore, such capillar system works as focusing lens. Assuming perfect overlap, the focal spot size is determined by the spot size from each individual channel capillary, which depends on the channel size r_0 , the output focal length f_{out} (Fig. 4) and the local divergence β [55,58]:

$$\Delta f \approx [r_0^2 + (f_{\text{out}}\beta^2)]^{1/2}. \quad (5)$$

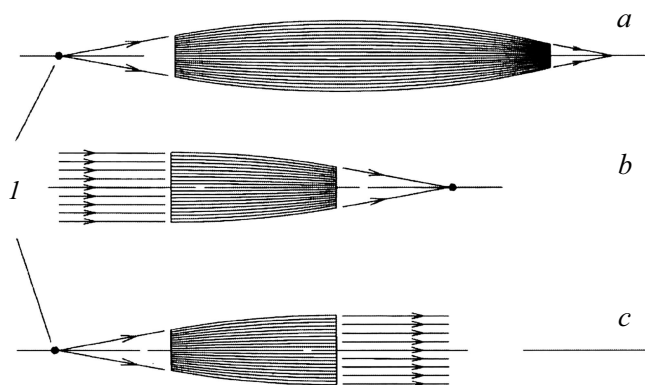


Figure 5. X-ray polycapillary optics: focusing lens „point source–focus“ (a); focusing half-lens „parallel beam–focus“ (b); half-lens „point source–quasi-parallel beam“ (c) (*I* — X-ray point source) [54].

The divergence at the capillary output β is not equal to zero, but is approximately determined by the critical angle and, therefore, depends on the X-ray energy. In general, the local divergence β is $\sim 1.3\theta_c$. The coefficient 1.3 is an experimentally determined parameter that arises from the fact that major portion of the beam has divergence less than the maximum divergence $2\theta_c$ created by reflection at the critical angle. The beam local divergence does not depend on the source size, although large sources cannot be effectively „captured“ by optics. The critical angle θ_c for radiation energy $E = 20$ keV is 1.5 mrad. At $\beta = 1.3\theta_c$ optics with $r_0 = 3.4\ \mu\text{m}$ and $f_{\text{foc}} = 9$ mm has a predicted spot size of $18\ \mu\text{m}$ [55].

The use of capillar lens makes it possible to increase the radiation density G , i.e. the ratio of the radiation density in the focal spot of the lens to the radiation density created by the source without lens at the same distance from the source as the focal spot [9]:

$$G = (L\Delta\phi/\Delta f)^2 T, \quad (6)$$

where T is transmission coefficient of the polycapillary of the system is not small ($T > 10\%$), $\Delta\phi$ is angular aperture of the polycapillary at the input, L is lens length.

$G = 2500$ [59] and $G = 2970$ [60] have been reported for the glass polycapillary, which is much larger than the gain of the conical monocapillary ($G = 960$ at $E = 6$ keV) measured by the authors of paper [26].

Along with the polycapillary lens, which makes it possible to focus radiation from a finite source (X-ray tube), the capillary half-lens is used, which is capable to focus the parallel beam (for example, SR beam) or transforming it into quasi-parallel beam with divergence within double critical angle (Fig. 5).

It has been shown that polycapillary focusing lens together with X-ray microfocus tube can be used in medicine [58,61], X-ray microscopy [62,63], to obtain X-ray phase contrast image [64], for microdiffraction [65,66], X-ray fluorescence analysis [60,67–69] (Fig. 6).

Information about the two-dimensional (2D) distribution of elements can be obtained by raster scanning of the sample with respect to primary X-rays focused into a microbeam. Today, this method, often referred to as scanning X-ray fluorescence microscopy (SXFM), is the most popular method for research relating the arts and cultural heritage. However, problems may arise here due to the large size of the objects of study (for example, paintings), which are often difficult to deliver to the laboratory from museums or repositories. Therefore, mobile units have been developed using polycapillary focusing optics for field studies (*in situ*). The demand for such instruments has stimulated the production of commercial instruments [70]. Bruker Nano GmbH (Berlin, Germany) consistently developed three options of experimental units: ARTAX [71], Tornado M4 [72] and M6 Jetstream [70]. They use microfocus X-ray tubes and polycapillary focusing optics, which provide a spatial resolution at least $100\ \mu\text{m}$. The ARTAX system was developed primarily for local X-ray fluorescence analysis of cultural heritage; it can also be used for fluorescence visualization [71], but the scanning area is limited to $5 \times 5\ \text{cm}^2$. Thus, ARTAX is not suitable for studying large objects. In Tornado M4 the maximum size of the test sample is $20 \times 16\ \text{cm}$, and for the Bruker M6 Jetstream, the scanning area reached $80 \times 60\ \text{cm}^2$; in this case a stationary sample is scanned with X-ray beam, which provides possibilities for the massive objects study. Apparently, this is the reason for its increased demand [73–78].

Polycapillary half-lens are used for efficient focusing of a quasi-parallel SR beam with energy in the range of 2–30 keV to small spots (diameter 10–50 μm) [79–85]. Polycapillary half-lens are also successfully used in confocal X-ray optics.

2.3. Confocal X-ray optics

One of the tasks facing the researchers is the need to analyze objects with a non-uniform distribution of elements not only over the surface, but also through depth, in

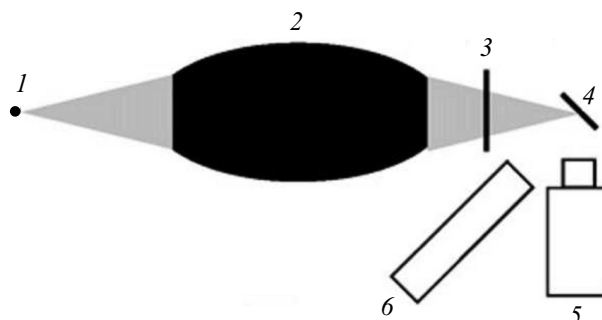


Figure 6. Scheme of experimental setup for X-ray fluorescence analysis (*1* — anode of microfocus X-ray tube, *2* — polycapillary lens, *3* — filter, *4* — sample, *5* — detector, *6* — optical microscope) [60].

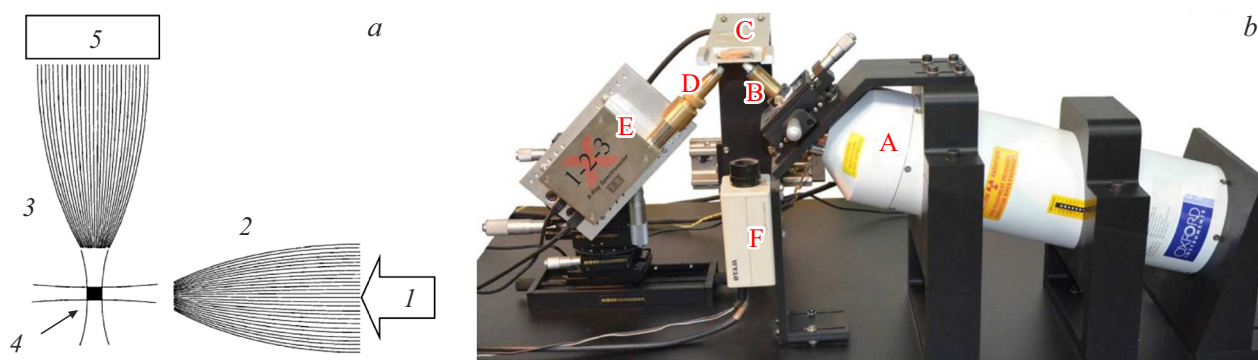


Figure 7. (a) Scheme of X-ray confocal optics using SR: 1 — quasi-parallel SR beam; 2 — focusing polycapillary half lens; 3 — collimator polycapillary half lens directing fluorescent radiation from the confocal volume 4 to the detector 5. (b) Laboratory fluorescence spectrometer [101]: A — X-ray tube, B — focusing polycapillary lens, C — sample holder, D — collimating polycapillary half lens, E — semiconductor detector, F — CCD camera.

the particular case — of objects with layered structure. To solve this problem, in the early 1990s, Gibson and Kumakhov [53,86] proposed the method of confocal X-ray fluorescence spectroscopy (CXFS) [87–90]. The essence of the method is the use of spatial filtering to cut off radiation from a part of the sample out of focus (background illumination). In CXFS, in addition to the optics that focuses the primary radiation, an additional optical element is used, installed between the sample and the detector, which ensures the local selection of fluorescent radiation from the sample volume. In this case, fluorescent radiation is recorded, which comes only from the volume determined by the area of overlap of the optical foci of the X-ray optics elements, the so-called confocal volume. For this purpose, the polycapillary lens or half-lens [91] is usually used, which makes it possible to collect fluorescent radiation and direct it to the input window of the detector (Fig. 7, a).

Although the use of SR together with confocal XRF showed its long-term benefits [92–94], the limited availability of tools stimulated research in configurations with laboratory sources [89,95–102] (Fig. 7, b). Desktop X-ray sources emit much fewer photons than SR sources, which results in a lower element sensitivity by about one–two orders [103].

However, the difference in the brightness of the radiation sources has practically no effect on the method resolution. For example, for optical configuration formed by two polycapillary lens, for a laboratory instrument [104] the focal spot size was experimentally estimated as equal to $10\ \mu\text{m}$ at energy of $17.4\ \text{keV}$ ($\text{Mo K}\alpha$), and the resolution through depth varied from 22.6 to $13.7\ \mu\text{m}$ as X-ray energy changed from 5.4 to $11.4\ \text{keV}$, respectively (with energy increasing the TER critical angle decreases and, thus, radiation can be collected from smaller volume) using SR the authors of paper [105] managed to obtain a confocal volume equal to $15 \times 15 \times 20\ \mu\text{m}^3$ at $E = 17.2\ \text{keV}$. Note that the lateral resolution and resolution through depth are determined by the parameters of the focusing optics

installed in front of the sample and the detector, respectively.

The CXFS method has found application in various fields of researches. Resolution through depth plays a fundamental role when the sequence of layers consisting of different elements is unknown, and if, moreover, this sequence varies along the surface of the sample. Therefore, the method was used in the study of layer structures, such as paintings [106–116] and arts and crafts [117–119], multilayer semiconductor devices [120]. The method can be used to study mechanism parts [121], corrosion of metals [122,123], *in operando* energy converters [124,125], interfaces „liquid/solid“ [126]. The possibility of using the CXFS method in medicine [127–129], geology [130–132], archeology [133–135], criminology [136,137], study of printed goods [138], environmental studies [139], studies of near-Earth space and outer space [140] is shown, as well as in pharmaceuticals since the mapping of various complexes in a tablet is an important problem for manufacturing quality control, as well as to detect counterfeits. For example, it was shown [141] that it is possible to measure the distribution of several inorganic elements (Zn, Fe, Ti, Mn, Cu) down to a depth of several hundred microns below the tablet surface, excluding „interference“ in the analysis of the tablet coating, and in the same experiment to measure the coating thickness.

Sometimes it is necessary to know the thickness and composition of the outer layer (shell) of the object of study. For example, in the paper [142] outer layer was found in rice grains, which is about $80\ \mu\text{m}$ thick and enriched in metals. Therefore, in regions that are affected by heavy metals and other poisonous pollution elements, the preparation of rice dishes needs abundant water for rice treatment and cooking.

3. Focusing porous X-ray optics

3.1. Voltaire I geometry

The idea of using TER for X-ray optics was born in 1960 when R. Giacconi and B. Rossi evaluated the possibility of creating a truncated parabolic X-ray reflector [143] capable of focusing a paraxial X-ray beam without spherical aberration.

The parabolic shape, however, cannot be used to build TER based telescopes, as they would be affected by strong coma-aberration; as a result, the field of view of the optics will be small to create any image in the focal plane.

In 1952 Voltaire demonstrated a double mirror system in which the X-rays used for image formation were subjected to two successive reflections from a paraboloid, and then a hyperboloid [6]. The advantage of a double mirror system is the reduction of optical aberrations such as coma and hence the angular resolution improvement. But due to the remoteness of most astronomical objects the radiation intensity at the input of the X-ray telescope is, as a rule, extremely low. Since the grazing angle shall be less than the TER critical angle, the effective area of a single mirror is very small. To increase the effective area of the telescope, several coaxial and confocal mirrors with decreasing radii („mirror shells“) are used, nested into each other like a Russian nesting doll, with the grazing angle decreasing from the outer shell to the inner one (Fig. 8) [144,145].

High angular resolution comes at a cost: mirrors must have a precise surface shape with high quality workmanship and rigid mounting. These requirements lead to thick shells, high weight and high costs. On the other hand, the transition to lighter thin mirror shells makes the optics less rigid. Such stiffness decreasing makes the mirror more susceptible to random loads and distortion, which can degrade its shape. Therefore, the manufacturing and assembly of thin light elements of X-ray focusing optics with high angular resolution is a significant and unique technical problem for modern astrophysics [146].

For future X-ray telescopes it is necessary to reduce the weight and volume density of the mirror shells packing, while maintaining efficiency, fine alignment, and structural stiffness.

It has been shown [147] that glass microporous material and milliporous silicon structures form „viable“ components of X-ray optics. Both technologies are based on commercially available products and technological processes. Demonstration lens tests have shown that their efficiency can be acceptable for light, compact glass optics and lens with higher resolution and efficiency in case of the silicon optics.

Silicon porous optics

It has been shown [7,144,147–150] that silicon porous optics (SPO) can serve as a new technology for creating the next generation of X-ray telescopes. The choice of silicon as a material for focusing optics is not accidental: silicon has a low density (2.3 g/cm^3), good strength, a low

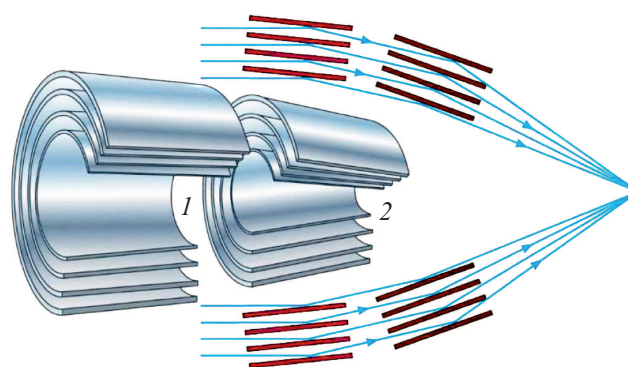


Figure 8. Path of X-rays in multilayer Voltaire I mirror. When focusing, the rays are successively reflected from the parabolic (1) and hyperbolic (2) surfaces of each mirror shell.

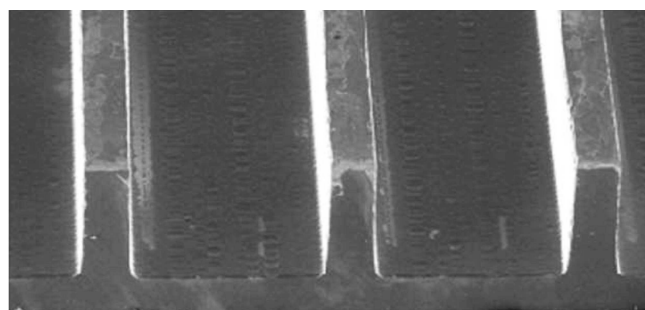


Figure 9. Section of silicon wafer with stiffeners 0.17 mm wide, spacing 1 mm and membrane 0.17 mm thick [7].

thermal coefficient of linear expansion, and can be polished with extremely high quality. The manufacturing process of silicon wafers is optimized by the semiconductor industry, which facilitates the production of mirrors with specified parameters.

In the polished rectangular silicon wafers the grooves are cut to form a ribbed structure (Fig. 9). They have two main functional parts: a membrane that acts as a mirror, and ribs for connecting several plates (Fig. 10, a), the distance between which can be $\sim 1 \text{ mm}$. One wall of each pore is used as a working (reflecting) surface, and the side walls give the structure a special rigidity. To improve the reflectivity of the mirrors, their working surface is covered with a metal film. The mirror surface shape required for Voltaire I optics (or its conical approximation) is obtained by bending and stacking several mirrors on top of each other, forming a SPO mirror block (Fig. 10, b). The important point is that the plates are connected without any adhesive by hydrophilic bonding of the activated surfaces. Then, in order to obtain the Voltaire I configuration, two SPO blocks are located one after the other, aligned and connected into SPO mirror module (Fig. 10, c). The aperture of X-ray telescope is filled with hundreds of mirror modules combined into sectors [7] (Fig. 10, d, e) or a system of

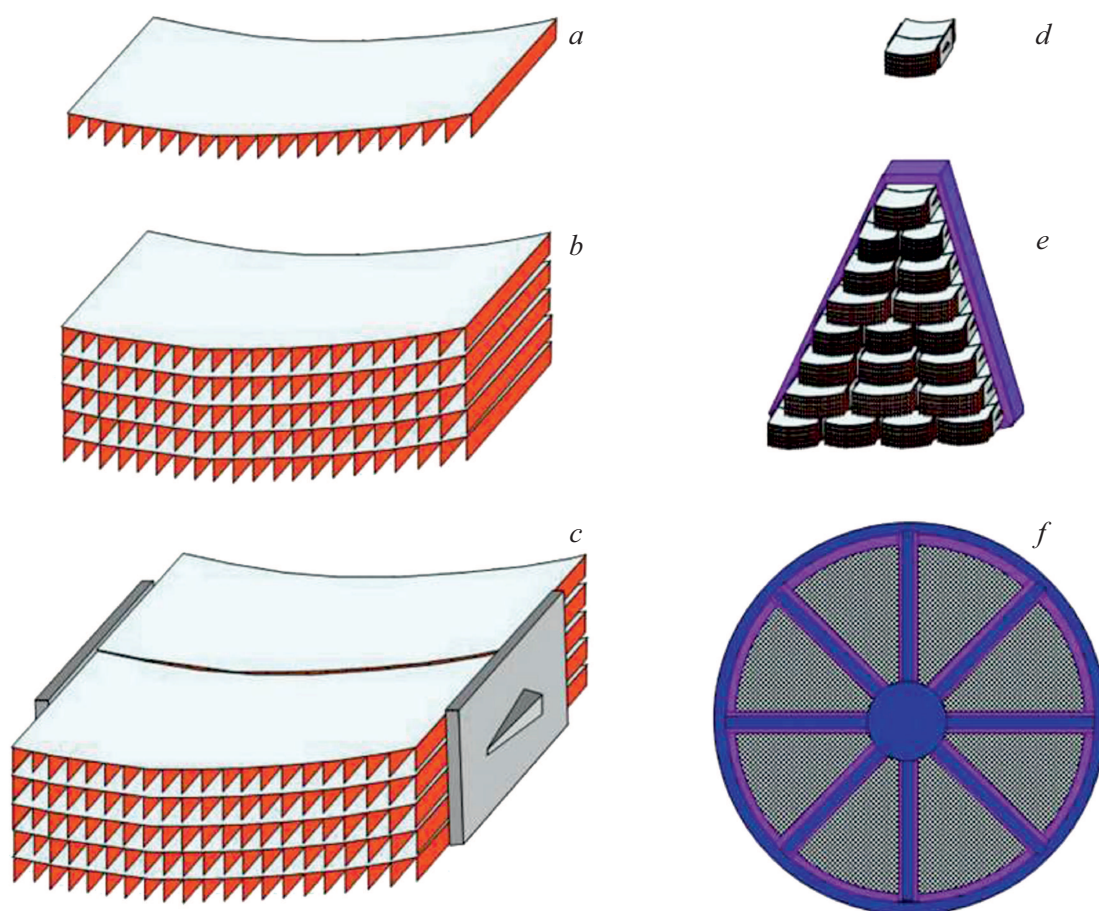


Figure 10. Illustration of SPO manufacturing technology. Bent mirror plates with stiffeners (*a*) are combined into mirror blocks (*b*); two SPO blocks are connected with clamps to form mirror module of Voltaire I optics (*c, d*); modules fill the sectors (*e*) forming the telescope lens (*f*) [7].

concentric rings [144]. In this way, structural rigidity can be achieved through a monolithic porous structure of optical modules that are individually aligned into the optical module, replacing the approach for mounting the separate shells used in more traditional X-ray optical technologies. This allows significant decreasing of the substrate thickness resulting in a denser packing of mirror shells, thus increasing the effective collection surface without detriment to optics rigidity and shape accuracy.

Glass microporous optics

One of the most promising approaches for creating light and efficient focusing optics is the use of microporous (microchannel) plates. The width of the holes in them are so small (20–100 μm) that the substrate thickness, i.e. the mirror length can be small, from hundreds of micrometers to tens of millimeters. As a result, optics with micropores can be lighter than traditional X-ray telescope optics by more than ten times. Thus, microporous optics, provided that its angular resolution is improved, can be used for low-weight telescopes with a large effective area [151].

Microchannel plates (MCP) [7,148,152–157] are made from polished glass blocks surrounded by cladding glass

with a lower melting point. The blocks are drawn out into thin fibers. These fibers are combined into a circular or square array, which is drawn out again to form a multifiber. To create radially packed MCPs the multifibers are arranged in concentric rings and fused at high temperature and pressure to form a bunch. MCP blanks few millimeters thick are cut from the bunch before the soluble glass core is etched with acid, resulting in the desired structure of micropore with the desired cross-section, in which the pore walls are formed by the cladding glass. MCPs are coated with a thin layer of an element with a high Z (e.g. platinum, iridium, etc.) to increase the TER efficiency. Depending on the application the optics can be thermally given a spherical shape of a certain radius. Therefore, the technology can be used to simulate two surfaces of revolution that make up the conical approximation of Voltaire I geometry for X-ray visualization [154,155,158]. This requires two plates aligned so that the channels in the first plate match those in the second plate and are fixed together to form the structure shown in Fig. 11. The plates should be bent to spherical shape, where the radius of curvature of the second plate is 1/3 of the radius of the first plate. X-rays from the

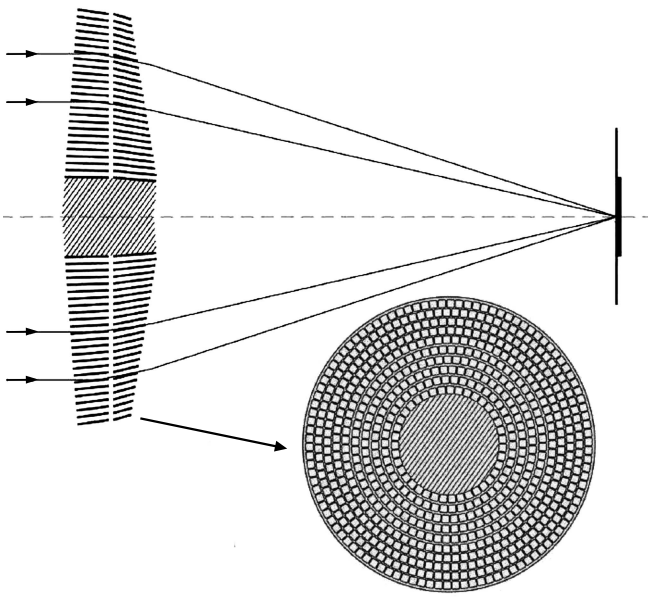


Figure 11. Voltaire I optics can be implemented using a large number of rectangular pores arranged in concentric circles around the core [148].

source located at a great distance are reflected sequentially by the first and second plates, and the image is formed at focal length of $1/4$ of the radius of curvature of the first plate [7,154]. Such optics can provide a large effective area with a very small weight [154].

It was expected to implement MCP in the flight program of the *BepiColombo* mission and the *SVOM* mission [159]. For the radially packed MCP optics of the *SVOM* mission with square pores $20\mu\text{m}$ in the conical approximation of the Voltaire I geometry the focal length is 1 m, which is determined by the radii of curvature 4 and 1.33 m of the front and back plates of MCP tandem pair. The optics with a diameter of 210 mm is assembled from MCP tandem pairs, each of which is a sector of a circle. The tandems are arranged in three rings with different thicknesses (2.2 mm inner, 1.3 mm middle and 0.9 mm outer) to approach the ideal thickness profile, which increases the throughput of the telescope by maximizing the probability of single reflection in each MCP [159].

Silicon microporous optics

Silicon microporous optics is so called microelectromechanical systems (MEMS) using anisotropic wet etching of silicon wafers with surface orientation (110) [160]. Because they are manufactured based on lithography, the accurate pores are available in scale $1\mu\text{m}$. This type of microporous optics may be the lightest X-ray optics due to the small pores of high density. Since etching allows the production of a number of X-ray mirrors by one etching process, the technology has very low price.

MEMS microporous optics fabricated by deep reactive ion etching is characterized by high roughness of the side walls of microchannels (10–30 nm). To improve the

characteristics of three-dimensional MEMS microstructures, a combined use of dry and anisotropic wet etching [160] of silicon microchannel X-ray optics was proposed in the paper [161]: the first process is to give the microstructure the required optical shape, the second — to obtain smooth channel walls.

To reduce the roughness of the channel walls, the authors of paper [162, 163] used the method of hydrogen annealing at a temperature of 1000–1300°C. The root-mean-square surface roughness after hydrogen annealing can be extremely small (on the order of 0.1 nm).

The papers [164,165] describe the process of ultra-precise polishing to the roughness of $< 3\text{ nm}$ using an alternating magnetic field. The main factor determining the success of polishing is the effect of abrasive particles on the workpiece by the force of the magnetic field. It was found that the process is mainly controlled by the oscillations frequency and the magnetic field strength.

Obviously, to manufacture Voltaire I optics it is necessary to bend the microchannel plate into mirror block and connect two plates with different curvature radius. However, in the case of a silicon structure the elastic deformation is difficult due to the brittleness and rigidity of silicon. In this case, it is possible to use the technology of hot plastic deformation of silicon. The monocrystal silicon wafer can be plastically deformed into a three-dimensional shape by placing the wafer between concave and convex dies at high temperature ($> 700^\circ\text{C}$) [166]. The X-ray telescope using thin silicon wafers with many small pores as focusing optics can be the lightest one ever manufactured [163].

3.2. Optics „lobster eyes“

Monitoring of large areas of the sky is of particular interest in X-ray astronomy due to the large variability in time of most X-ray sources. It is expected that wide-field X-ray telescopes with focusing optics will become an important tool in future space astronomy projects. X-ray optics, proposed in the 70s by Schmidt [167] and Angel [168], provides an excellent opportunity to obtain a very wide field of view (1000 square degrees or more), while the commonly used classical Voltaire I grazing - incidence mirrors are limited to about 1° [8].

The two-dimensional Schmidt system consists of orthogonal stacks of flat foils arranged like a fan along the perimeter of two cylinders with radii R_1 , R_2 (Fig. 12, a). Angel optics can be considered as a special case of the Schmidt system, where both stacks lie in the same position but have the same radii $R_1 = R_2 = R$ (Fig. 12, b). At that, two stacks of mirrors form square pores (Fig. 12, c).

Here we will be interested in Angel's optics, which is commonly called „lobster eye“ (LE) optics and which forms a separate class of porous optics. The fact is that the eyes of lobsters and other crustaceans (shrimp, crayfish, etc.) are arranged differently than in most other animals: they do not refract, but reflect the incident light. That is, to focus light on the retina, not lens are used, which are

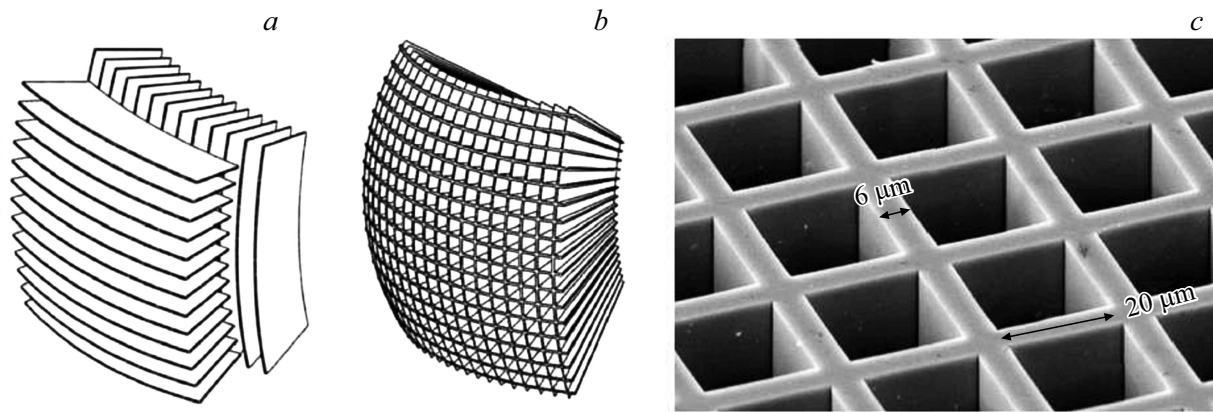


Figure 12. Two-dimensional focusing optics in geometry of Schmidt (a) and Angel (b). SEM image of micropores (c).

the crystalline lens of higher vertebrates, but many tiny channels with reflective inner walls and almost perfectly square section located on a spherical surface. Such system has an extremely high light sensitivity, which is practically unattainable with conventional lens.

Special interest in LE optics was shown by astrophysicists [8,169–174].

Microchannel plates with square pores and square packing (Fig. 12, c) are made by drawing out, melting and etching of the lead glass fibers [175]. The LE optics is a microchannel plate located on a sphere with radius R (Fig. 12, b, 13, a). However, in contrast to the MCP and MEMS optics considered above, in which the focus is formed by X-rays one time reflected in each plate, in the LE optics the focus is formed by rays successively reflected from adjacent (orthogonal) walls of the channel. These rays are concentrated on the focal surface with radius $R/2$. The LE lens generates a cruciform shape of the focus with branches resulting from photon reflections from one channel wall. As a result, the focus structure is a bright spot with a weaker cross and a much less intensive diffuse background formed by X-rays that passed through the lens without reflections (Fig. 13, b).

The disadvantage of the LE optics is the need for large-sized image-recording detectors mounted on the focal surface.

The geometric angular resolution $\Delta\theta_g$ can be estimated as the ratio of the channel size d to the focal length f ($f = R/2$):

$$\Delta\theta_g = 2d/R. \quad (7)$$

Finally, the field of view FoV of the lens with $N \times N$ channels is determined by the range of angles formed by all channels [176]:

$$\text{FoV} \approx N(2d/R) = N\Delta\theta_g. \quad (8)$$

The size of the field of view depends only on the angular dimensions of the spherical optics and the detector. If the optics and detector cover a hemisphere, the field of view

is the entire sky. Therefore, such optics is ideal for very wide applications in astronomy, despite the low resolution.

If a parallel beam is incident on the LE lens, the aperture is limited by a square with a side equal to $2R\theta_c$. Therefore, the largest achievable effective area is given by the formula [176]:

$$(A_{\text{eff}})_{\text{max}} = 4(R\theta_c)^2. \quad (9)$$

To obtain the most effective field of view, $\theta_c \approx (180/\pi)(8^{1/2} + 1)d/L$ degrees (L is channel axial length) is required, therefore, when using a high-density coating material, such as iridium, at X-ray energy of 1 keV, the optimal ratio is $L/d = 50$. Microcapillary plates are produced with standard pore sizes, usually 20 or 40 μm , so that the thickness of the plates is in the range 1–2 mm.

In the paper [177] all significant aberrations were identified, which limit the characteristics of microchannel plates with square pores used as X-ray LE optics. There are three intrinsic aberrations that limit the angular resolution. Spherical aberration depends on the aspect ratio (L/d) and gives the angular resolution $\Delta\theta_s = 32^{1/2}(d/L)^3$, the geometric size of pores limits the angular resolution to $\Delta\theta_g = d/f$, and diffraction limits the angular resolution to $\Delta\theta_d = 2\lambda/d$. Using the optimal aspect ratio $L/d = 50$ gives the spherical aberration limit $\Delta\theta_s \approx 9''$. In the absence of external aberrations, maximum angular resolution will be obtained if the pore size is chosen such that the geometric and diffraction limits are equal. In this case $d = (2\lambda f)^{1/2}$ is required, which gives $\Delta\theta_g = \Delta_d = (2\lambda/f)^{1/2}$. For $E = 1$ keV, $f = 1$ m and $d = 50 \mu\text{m}$ $\Delta\theta_g = \Delta\theta_d = 10''$. If we combine the spherical, geometric and diffraction limits, we get the proper angular resolution $(\Delta\theta_g^2 + \Delta\theta_d^2 + \Delta\theta_s^2)^{1/2} = \Delta\theta_i \approx 17''$. Repeating this calculation for $f = 0.3$ m and using the same value of L/d , we get the optimal pore size $d = 27 \mu\text{m}$, $\Delta\theta_g = \Delta\theta_d = 19''$ and the total limit of angular resolution $\Delta\theta_i = 28''$.

The pore size d of the available glass microchannel plates is in good agreement with the limits of the optimal angular resolution of the LE geometry for X-ray telescope

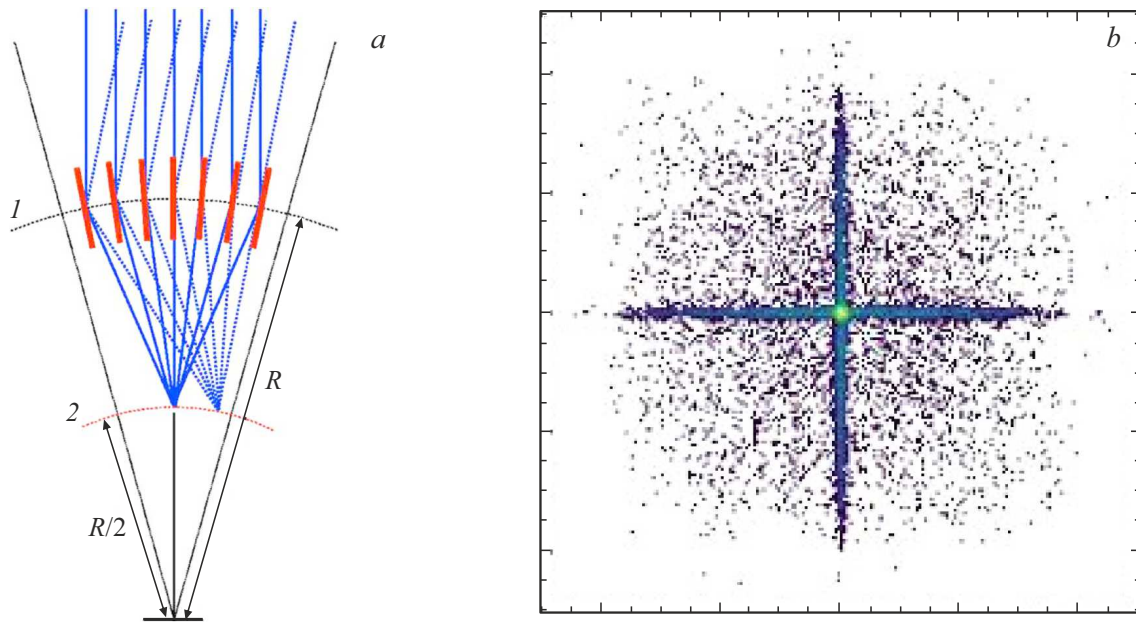


Figure 13. Diagram of the LE optics showing X-ray mirror cells *1* mounted on spherical surface with radius R and focal surface *2* at focal length $R/2$. X-ray radiation from different positions of sources in the sky is focused at different places on the focal surface (*a*). Cruciform focus of the LE optics (*b*) [174].

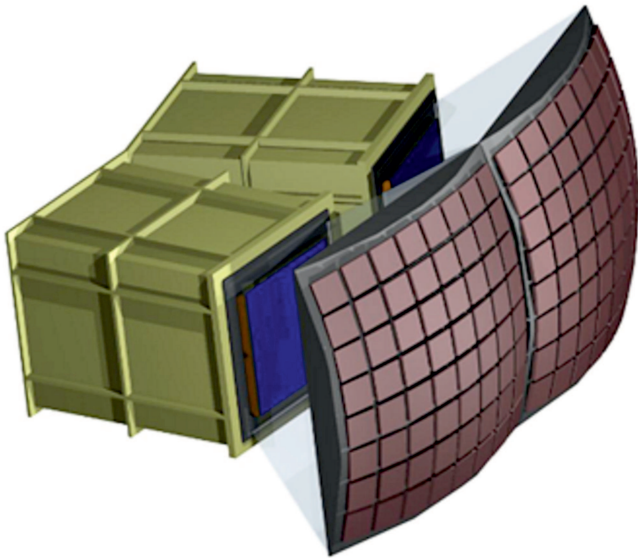


Figure 14. General view of two of the four modules of LE optics of SXI scanner of the THESEUS mission [189] (see text).

in the energy range 0.1–10 keV. They can be made with L thickness in the range of 0.9–4 mm, which gives the optimal $L/d \sim 50$ value for efficient X-ray imaging in the same energy range. When imaging in a narrow field of view, the native angular resolution limit will be 10–20'', and for shorter focal lengths, more suitable for applications requiring a wide field of view, the limit will be in the range of 20–30'' [177].

However, the angular resolution is also highly dependent on manufacturing errors and external factors. Therefore, a number of papers have been devoted to optimizing the optical characteristics of the LE lens [173,174,178–182]. For example, the authors of the paper [178] proposed ways to optimize the technology of glass preparation and drawing out, monitoring of production processes and metrology, the processes of fiber laying, etching of the glass core and thermal bending of microchannel plates were improved, as well as methods for coating the channel walls with reflective film. To improve the angular resolution paper [180] recommended to use thermal control of the LE optics. To obtain a high aspect ratio, radially oriented rectangular channels, to reduce the misorientation of the channels and the roughness of their surfaces (the latter are the main factors in the limiting resolution and reflectivity of porous optics), the authors of the papers [181,182] propose the use of X-ray lithography as a possible competing technology for the microporous optics manufacturing.

The LE optical system was used in several scientific missions aimed at monitoring the entire sky: *Lobster-ISS* [183], *AXIOM* [184], *STORM* [185,186], *SMILE* [187], *SVOM* [188], *THESEUS* [189].

For example, the optics aperture of the X-ray scanner SXI of the *THESEUS* mission is formed by the array of 8×8 microchannel plates with square pores $40 \times 40 \text{ mm}^2$ each (Fig. 14). Microchannel plates are mounted on a spherical frame with a curvature radius of 600 mm. The focal plane of each scanner module is a spherical surface with a curvature radius of 600 mm, located at a distance of 300 mm (focal length) from the optics aperture. The detectors for each

module consist of 2×2 array of large format detectors tilted to approach the spherical focal surface.

Conclusion. Conclusions and perspectives

It should be stated that today the most common and convenient method of focusing the primary X-ray radiation is the use of capillary and polycapillary X-ray optics. Due to their moderate resolution, polycapillary elements provide high intensity and are often used as X-ray concentrators with synchrotrons and X-ray tubes. In combination with microfocussing X-ray tubes, capillary lens make it possible to create compact instruments for non-destructive local elemental analysis.

One of the possible ways of further development of polycapillary optics may be to give it the function of imaging optics. Defect microscopy [190] was recently proposed, using the natural defects of polycapillary structures, such as broken, missing, or slightly larger capillaries. It was demonstrated that such defects, violating the periodicity of capillary gratings, result directly to the formation of multiple X-ray images of the object placed at the focus of polycapillary optics. Multiple images can be analyzed using the coding aperture principle and promise to provide a spatial resolution of $0.5 \mu\text{m}$. The method is very promising, but for practical applications it requires complex fabrication of special X-ray optics with intentionally introduced defects. Therefore, submicron coding aperture microscopy was proposed in the paper [191] using an external periodic mesh located on the output surface of polycapillary optics.

The achievements in the field of creating light X-ray optics in the Voltaire I geometry based on microporous plates are impressive. However, much work remains to be done here to significantly improve the angular resolution. Besides, there is the problem of aligning two microporous plates of different curvature with a large number of channels. Therefore, the new compact and light glass microporous X-ray optics proposed by the authors of the papers [192,193], which using femtosecond laser radiation and wet etching forms Voltaire I system in a single glass substrate without its bending and the need for alignment, may be promising.

Wide-angle X-ray „lobster eye“ optics reached a level that allows its successful use in orbiting telescopes. Recent new developments have shown that „lobster eye“ optics is also suitable for X-ray visualization of non-astronomic objects [194], and can be used in medicine, security and counter-terrorism system. For example, the portable device LEXID („Lobster-Eye“ X-ray Inspection Device), developed by Physical Optics Corporation (POS) under the order of the US Department of Homeland Security, is based on the registration of X-ray radiation scattered by the object under study, and can see through concrete walls and steel barriers several centimeters thick from a distance of up to 2.5 m [195]. The device is primarily designed for customs officers.

Another development of the same company is the device LEXIUS — an underwater X-ray scanner/reflectometer system to obtain high-quality images of mines and other objects hidden by bottom sediments.

Conclusion: focusing X-ray capillary and porous optics are widely used high-effective techniques that have the potential for further development and improvement.

Funding

The study was performed with support of the Ministry of Science and Higher Education during works performing under the Government Task of FSRC „Crystallography and Photonics“ of RAS.

References

- [1] *Ice G.E., Budai J.D., Pang J.W.L.* // Science. 2011. V. 334. N 6060. P. 1234.
- [2] *Schmahl G., Rudolph D., Schneider G., Guttman P., Niemann B.* // Optik. 1994. V. 97. N 4. P. 181.
- [3] *Guttman P., Zeng X., Feser M., Heim S., Yun W., Schneider G.* // J. Phys.: Conf. Ser. 2009. V. 186. N 1. P. 012064.
- [4] *Howells M., Jacobsen C., Warwick T., Bos A.* // Principles And Applications of Zone Plate X-Ray Microscopes. Science of Microscopy. NY.: Springer, 2007. V. 2. P. 835.
- [5] *Wolter H.* // Ann. Phys. 1952. B. 10. S. 94.
- [6] *Wolter H.* // Ann. Phys. 1952. B. 10. S. 286.
- [7] *Bavdaz M., Collon M., Beijersbergen M., Wallace K., Wille E.* // X-ray Opt. Instrum. 2010. V. 2010. ID 295095.
- [8] *Priedhorsky W.C., Peele A.G., Nugene K.A.* // Mon. Not. Roy. Astron. Soc. 1996. V. 279. N 3. P. 733.
- [9] *Dabagov S.B.* // UFN. 2003. V. 173. N 10. P. 1083 (in Russian).
- [10] *Furuta K., Nakayama Y., Shoji M., Kaigawa R., Hanamoto K., Nakano H., Hosokawa Y.* // Rev. Sci. Instrum. 1993. V. 64. N 1. P. 135.
- [11] *Wang L., Rath B.K., Gibson W.M., Kimball J.C., MacDonald C.A.* // J. Appl. Phys. 1996. V. 80. N 7. P. 3628.
- [12] *Chen G.J., Cerrina F., Voss K.F., Kim K.H., Brown F.C.* // Nucl. Instrum. Methods Phys. Res. A. 1994. V. 347. N 1–3. P. 407.
- [13] *Ullrich J.B., Kovantsev V.E., MacDonald C.A.* // J. Appl. Phys. 1993. V. 14. N 10. P. 5933.
- [14] *Arkad'ev V.A., Kolomijtsev A.I., Kumakhov M.A., Ponomarev I.Yu., Khodev I.A., Chertov Yu.P., Shakhparonov I.M.* // UFN. 1989. V. 157. № 3. P. 529 (in Russian).
- [15] *MacDonald C.A., Gibson W.M.* // X Ray Spectrom. 2003. V. 32. P. 258.
- [16] *Suparmi Cari, Wang L., Wang H., Gibson W.M., MacDonald C.A.* // J. Appl. Phys. 2001. V. 90. N 10. P. 5363.
- [17] *Storizhko V.E., Ilyashenko M.V., Molodkin V.B., Gaevsky A.Yu., Denisenko V.L., Denisenko O.I., Vershinsky S.A.* // Uspekhi fiz. met. 2010. V. 11. P. 1. (in Russian)
- [18] *Bilderback D.H.* // X-Ray Spectrom. 2003. V. 32. P. 195.
- [19] *Charnley N.R., Potts P.J., Long J.V.P.* // J. Anal. At. Spectrom. 1994. V. 9. N 11. P. 1185.
- [20] *Zeng X., Diewer F., Feser M., Huang C., Lyon A., Tkachuk A., Yun W.* // Appl. Opt. 2008. V. 47. N 13. P. 2376.

- [21] Bjeoumikhov A., Bjeoumikhova S., Wedell R. // Part. Part. Syst. Charact. 2005. V. 22. N 6. P. 384.
- [22] De Nolf W., Janssens K. // Surf. Interface Anal. 2010. V. 42. N 5. P. 411.
- [23] Snigireva I., Snigirev A. // J. Environ. Monit. 2006. V. 8. N 1. P. 33.
- [24] Thiel D.J., Bilderback D.H., Lewis A., Stern E.A. // Nucl. Instrum. Methods Phys. Res. A. 1992. V. 317. N 3. P. 597.
- [25] Bilderback D.H., Hoffman S.A., Thiel D.J. // Science. 1994. V. 263. N 5144. P. 201.
- [26] Hoffman S.A., Thiel D.J., Bilderback D.H. // Nucl. Instrum. Methods Phys. Res. A. 1994. V. 347. N 1–3. P. 384.
- [27] Vincze L., Janssens K., Adams F., Rindby A., Engstrijm P., Riekel C. // Adv. X-Ray Anal. 1999. V. 41. P. 252.
- [28] Balaic D.X., Barnea Z., Nugent K.A., Garrett R., Varghese R.F., Wilkins S.W. // J. Synchrotron Rad. 1996. V. 3. P. 289.
- [29] Chen J., Wu C., Tian J., Li W., Yu S., Tian Y. // Appl. Phys. Lett. 2008. V. 92. N 23. P. 233104.
- [30] Sorrentino A., Nicolás J., Valcárcel R., Chichón F.J. // J. Synchrotron Rad. 2015. V. 22. N 4. P. 1112.
- [31] Huang R., Szebenyi T., Pfeifer M., Woll A., Smilgies D.-M., Finkelstein K., Dale D., Wang Y., Vila-Comamala J., Gillilan R., Cook M., Bilderback D.H. // J. Phys.: Conf. Ser. 2014. V. 493. P. 012034.
- [32] Engström P., Larsson S., Rindby A., Stocklassa B. // Nucl. Instrum. Methods Phys. Res. B. 1989. V. 36. N 2. P. 222.
- [33] Merkle A., Gelb J., Lavery L. // Microsc. Microanal. 2013. V. 19. N S2. P. 1314.
- [34] Müller M., Mey T., Niemeyer J., Mann K. // Opt. Express. 2014. V. 22. N 9. P. 23489.
- [35] Benk M., Bergmann K., Schäfer D., Wilhein T. // Opt. Lett. 2008. V. 33. N 20. P. 2359.
- [36] Vincze L., Somogyi A., Osan J., Vekemans B., Török S., Janssens K., Adams F. // Anal. Chem. 2002. V. 74. N 5. P. 1128.
- [37] Bartoll J., Röhrs S., Erko A., Firsov A., Bjeoumikhov A., Langhoff N. // Spectrochim. Acta B. 2004. V. 59. N 10–11. P. 1587.
- [38] Limburg K.E., Lochet A., Driscoll D., Dale D.S., Huang R. // X-ray Spectrom. 2007. V. 36. N 5. P. 336.
- [39] Lopes R.T., Lima I., Pereira G.R., Perez C.A. // Pramana. 2011. V. 76. N 2. P. 271.
- [40] Mroczka R., Żukociński G., Lopucki R. // Proc. SPIE. 2017. V. 10235. P. 10235OE.
- [41] Lind Q.C., De Nolf W., Janssen K., Salbu B. // J. Environ. Radioact. 2013. V. 123. P. 63.
- [42] Wang J., Chen-Wiegart Y., Wang J. // Nat. Commun. 2014. V. 5. Art. 4570.
- [43] Merkle A., Gelb J. // Microscopy Today. 2013. V. 21. N 2. P. 10.
- [44] Tan C., Daemi S.R., Heenan T.M.M., Iacoviello F., Leach A., Rasha L., Jervis R., Brett D., Shearing P. // J. Electrochem. Soc. 2020. V. 167. N 6. P. 060512.
- [45] Li R., Cornaby S., Kamperman M., Smilgies D.M. // J. Synchrotron Rad. 2011. V. 18. N 5. P. 697.
- [46] Sirenko A.A., Kazimirov A., Huang R., Bilderback D.H., O'Malley S., Gupta V., Bacher K., Ketelsen L.J.P., Ougazaden A. // J. Appl. Phys. 2005. V. 97. N 6. P. 063512.
- [47] Li F., Liu Z., Sun T. // J. Appl. Cryst. 2016. V. 49. N 2. P. 627.
- [48] Kazimirov A., Bilderback, Huang R., Sirenko A., Ougazaden A. // J. Phys. D: Appl. Phys. 2004. V. 37. N 4. P. L1.
- [49] Pantell R.H., Chung P.S. // IEEE J. Quant. Electron. 1978. V. 14. N 9. P. 694.
- [50] Bushuev V.A., Orudzhaliyev M.N., Kuzmin R.N. // ZhTF. 1989. V. 59. N 11. P. 153.
- [51] Kumakhov M.A. // Nucl. Instrum. Methods Phys. Res. B. 1990. V. 48. N 1–4. P. 283.
- [52] Kumakhov M.A., Komarov F.F. // Phys. Rep. 1990. V. 191. N 5. P. 289.
- [53] Kumakhov M.A. // X-ray Spectrom. 2000. V. 29. N 5. P. 343.
- [54] Gao N., Janssens K. Polycapillary X-ray optics/ in: X-Ray Spectrometry: Recent Technological Advances, Wiley, Chichester, 2004. P. 89.
- [55] MacDonald C.A. // X-Ray Opt. Instrum. 2010. V. 2010. Art. 867049.
- [56] Bolotokov A., Zaitsev D., Lyutsau A., Shcherbakov A. // Analitika. 2012. № 4 (in Russian). P. 14.
- [57] Beloglazov V., Langhoff N., Tuchin V., Bjeoumikhov A., Bjeoumikhova Z., Wedel R., Skibina N., Skibina Y.S., Chainikov M. // J. X-Ray. Sci. Technol. 2005. V. 13. N 4. P. 179.
- [58] MacDonald C.A., Petrucci J.C. // J. Phys.: Conf. Ser. 2016. V. 776. P. 012001.
- [59] Wegrzynek D., Mroczka R., Markowicz A., Chinea-Cano E., Bamford S. // X-Ray Spectrom. 2008. V. 37. N 6. P. 635.
- [60] Sun T., Liu Z., Li Y., Wang G., Zhu G., Ding X., Xu Q., Liu H., Luo P., Pan Q., Lin X., Teng Y. // Spectrochim. Acta B. 2009. V. 64. N 11–12. P. 1194.
- [61] MacDonald C.A., Gibson W.M. // Proc. SPIE. 1995. V. 2519. P. 186.
- [62] Sun T., MacDonald C.A. // J. Appl. Phys. 2013. V. 113. P. 053104.
- [63] Sun T., MacDonald C.A. // J. X-Ray Sci. Technol. 2015. V. 23. N 2. P. 141.
- [64] Bashir S., Tahir S., MacDonald C., Petrucci J.C. // Opt. Commun. 2016. V. 369. P. 28.
- [65] Owens S.M., Ullrich J.B., Ponomarev I., Carter D.C., Sisk R.C., Ho J.X., Gibson W.M. // Proc. SPIE. 1996. V. 2859. P. 200.
- [66] MacDonald C.A., Owens S.M., Gibson W.M. // J. Appl. Cryst. 1999. V. 32. N 26. P. 160.
- [67] Gao N., Ponomarev I., Xiao Q.F., Gibson W.M., Carpenter D.C. // Appl. Phys. Lett. 1996. V. 69. N 11. P. 1529.
- [68] Gao N., Ponomarev I., Xiao Q.F., Gibson W.M., Carpenter D.C. // Appl. Phys. Lett. 1997. V. 71. N 23. P. 3441.
- [69] Yan Y., Gibson W.M. // Adv. X-Ray Anal. 2002. V. 45. P. 298.
- [70] Alfeld M., Pedroso J.V., van E. Hommes M., Van der Snickt G., Tauber G., Blaas J., Haschke M., Erler K., Dik J., Janssens K. // J. Anal. At. Spectrom. 2013. V. 8. N 5. P. 760.
- [71] Bronk H., Rhrs S., Bjeoumikhov A., Langhoff N., Schmalz J., Wedell R., Gorny H.-E., Herold A., Waldschläger U. // Fresenius J. Anal. Chem. 2001. V. 371. N 3. P. 307.
- [72] Haschke M., Rossek U., Tagle R., Waldschlager U. // Adv. X-Ray Anal. 2012. V. 55. P. 286.
- [73] Trentelman K., Bouchard M., Ganio M., Namowicz C., Patterson C.S., Walton M. // X-Ray Spectrom. 2010. V. 39. N 3. P. 159.
- [74] Trentelman K., Janssens K., van der Snickt G., Szafran Y., Woollett A.T., Dik J. // Appl. Phys. A. 2015. V. 121. P. 801.

- [75] Martins A., Albertson C., McGlinchey C., Dik J. // *Herit. Sci.* 2016. V. 4. P. 22.
- [76] Martins A., Coddington J., Geert van der Snickt, van Driel B., McGlinchey C., Dahlberg D., Janssens K., Dik J. // *Herit. Sci.* 2016. V. 4. P. 33.
- [77] Duivenvoorden J.R., Käyhkö A., Kwakkel E., Dik J. // *Herit. Sci.* 2017. V. 5. P. 6.
- [78] Hrnjića M., A. Hagen-Petera G., Bircha T., Barfod G.H., Sindbak S.M., Leshner C.E. // *Nucl. Instrum. Methods Phys. Res. B.* 2020. V. 478. P. 11.
- [79] Vincze L., Wei F., Proost K., Vekemans B., Janssens K., He Y., Yan Y., Falkenberg G. // *J. Anal. At. Spectrom.* 1997. V. 17. N 3. P. 177.
- [80] Hofmann A., Freinberg-Truffas C.A., Osens S.M., Padiyar S.D., MacDonald C.A. // *Nucl. Instrum. Methods Phys. Res. B.* 1997. V. 133. N 1-4. P. 145.
- [81] Proost K., Vincze L., Janssens K., Gao N., Bulska E., Schreiner M., Falkenberg G. // *X Ray Spectrom.* 2003. V. 32. N 3. P. 215.
- [82] Tomik B., Chwiej J., Szczerbowska-Boruchowska M., Lankosz M., Wójcik S., Adamek D., Falkenberg G., Bohic S., Simionovici A., Stegowski Z., Szczudlik A. // *Neurochem. Res.* 2006. V. 31. N 3. P. 321.
- [83] Sun T., Liu Z., He B., We S.i, Xie Y., Liu T., Hu T., Ding X. // *Nucl. Instrum. Methods Phys. Res. A.* 2007. V. 574. N 2. P. 285.
- [84] Sun T., Zhang M., Liu Z., Zhang Z., Li G., Ma Y., Du X., Jia Q., Chen Y., Yuan Q., Huang W., Zhu P., Ding X. // *J. Synchrotron Rad.* 2009. V. 16. N 1. P. 116.
- [85] Surowka A.D., Wrobel P., Adamek D., Radwanska E., Szczerbowska-Boruchowska M. // *Metallomics.* 2015. V. 7. N 11. P. 1522.
- [86] Gibson W.M., Kumakhov M.A. // *Proc. SPIE.* 1993. V. 1736. P. 172.
- [87] Nikolaev V.I., Chizhova E.V. // *Nauchnoe priborostroenie.* 2011. V. 21. № 2. P. 3.
- [88] Ding X., Gao N., Havrilla G. // *Proc. SPIE.* 2000. V. 4144. P. 174.
- [89] Nakano K., Tsuji K. // *J. Anal. At. Spectrom.* 2010. V. 25. N 4. P. 562.
- [90] Sun T., Ding X. // *Rev. Anal. Chem.* 2015. V. 34. P. 45.
- [91] Woll A.R., Agyeman-Budu D., Choudhury S., Coulthard I., Finnefrock A.C., Gordon R., Hallin E., Mass J. // *J. Phys.: Conf. Ser.* 2014. V. 493. P. 12028.
- [92] Chen G., Chu S., Sun T., Sun X., Zheng L., An P., Zhu J., Wu S., Du Y., Zhang J. // *J. Synchrotron Rad.* 2017. V. 24. N 5. P. 1000.
- [93] Hampai D., Cherepennikov Yu.M., Liedl A., Cappuccio G., Capitolo E., Iannarelli M., Azzutti C., Gladkikh Yu.P., Marcellia A., Dabagov S.B. // *JINST.* 2018. V. 13. N 4. P. C04024.
- [94] Bauters S., Tack P., Rudloff-Grund J.H., Banerjee D., Longo A., Vekemans B., Bras W., Brenker F.E., Van Silfhout R., Vincze L. // *Anal. Chem.* 2018. V. 90. N 3. P. 2389.
- [95] Tsuji K., Nakano K. // *X-Ray Spectrom.* 2007. V. 36. N 3. P. 145.
- [96] Nakazawa T., Tsuji K. // *X-Ray Spectrom.* 2013. V. 42. N 5. P. 374.
- [97] Kanngiesser B., Malzer W., Rodrigues A.F., Reiche I. // *Spectrochim. Acta B.* 2005. V. 60. N 1. P. 41.
- [98] Xiaoyan L., Zhihong W., Tianxi S., Qiuli P., Xunliang D. // *Nucl. Instrum. Methods Phys. Res. B.* 2008. V. 266. N 11. P. 2638
- [99] Mantouvalou I., Lange K., Wolff T., Gröttsch D., Lühl L., Haschke M., Hahn O., Kanngiesser B. // *J. Anal. At. Spectrom.* 2010. V. 25. N 4. P. 554.
- [100] Laclavetine K., Ager F.J., Arquillo J., Respaldiza M.Á., Scrivano S. // *Microchem. J.* 2016. V. 125. P. 62.
- [101] Xiang Z.J., Meng Z.Y., Liu Z.G., Pan K., Zhao W.G., Zhou P., Li Y. // *IOP Conf. Ser.: Mater. Sci. Eng.* 2020. V. 770. P. 012054.
- [102] Ingerle D., Swies J., Iro M., Wobrauschek P., Strelcić, Hradil K. // *Rev. Sci. Instrum.* 2020. V. 91. N 12. P. 123107.
- [103] Kanngiesser B., Malzer W., Mantouvalou I., Sokaras D., Karydas A.G. // *Appl. Phys. A.* 2012. V. 106. N 2. P. 325.
- [104] Tsuji K., Nakano K. // *J. Anal. At. Spectrom.* 2011. V. 26. N 2. P. 305.
- [105] Senkbeil T., Mohamed T., Simon R., Batchelor D., Di Fino A., Aldred N., Clare A.S., Rosenhahn A. // *Anal. Bioanal. Chem.* 2016. V. 408. N 5. P. 1487.
- [106] Seim C., Laurenze-Landsberg C., Schröder-Smeibidl B., Mantouvalou I., de Boerd C., Kanngiesser B. // *J. Anal. At. Spectrom.* 2014. V. 29. N 8. P. 1354.
- [107] Šmit Ž., Janssens K., Proost K., Langus I. // *Nucl. Instr. Methods Phys. Res. B.* 2004. V. 219–220. N 1. P. 35.
- [108] Kanngiesser B., Malzer W., Reiche I. // *Nucl. Instrum. Methods Phys. Res. B.* 2003. V. 211. N 2. P. 259.
- [109] Woll A.R., Bilderback D. H., Gruner S., Gao N., Huang R., Bisulca C., Mass J. // *Mater. Res. Soc. Symp. Proc.* 2005. V. 852. P. 281.
- [110] Woll A. R., Mass J., Bisulca C., Cushman M., Griggs C., Wazny T., Ocon N. // *Studies in Conservation.* 2008. V. 53. N 2. P. 93.
- [111] Malzer W. // *The Rigaku J.* 2006. V. 23. P. 40.
- [112] Reiche I., Müller K., Eveno M., Itié E., Menu M. // *J. Anal. At. Spectrom.* 2012. V. 27. N 10. P. 1715.
- [113] Reiche I., Müller K., Mysak E., Eveno M., Mottin B. // *Appl. Phys. A.* 2015. V. 121. N 3. P. 903.
- [114] Nakano K., Tabe A., Shimoyama S., Tsuji K. // *Microchem. J.* 2016. V. 126. P. 496.
- [115] Reiche I., Eveno M., Mülle K.r, Calligaro T., Pichon L., Laval E., Mysak E., Mottin B. // *Appl. Phys. A.* 2016. V. 122. N 11. P. 947.
- [116] Zhou P., Liu Z., Ma X., Meng Z., Xiang Z., Wang X., Sun T., Lin X., Li Y. // *Nucl. Instrum. Methods Phys. Res. B.* 2020. V. 464. P. 111.
- [117] Kanngiesser B., Mantouvalou I., Malzer W., Wolff T., Hahn O. // *J. Anal. At. Spectrom.* 2008. V. 23. N 6. P. 814.
- [118] Nakano K., Tsuji K. // *X-Ray Spectrom.* 2009. V. 38. N 5. P. 446.
- [119] Yi L., Qin M., Wang K., Lin X., Peng S., Sun T., Liu Z. // *Appl. Phys. A.* 2016. V. 122. N 9. P. 856.
- [120] Nakazawa T., Tsuji K. // *X-Ray Spectrom.* 2013. V. 42. N 3. P. 123.
- [121] Qin M., Y Li, Wang J., Han Y., Sun T., Liu Z. // *IOP Conf. Ser.: Mater. Sci. Eng.* 2017. V. 269. P. 012033.
- [122] Nakano K., Akioka K., Doi T., Arai M., Takabe H., Tsuji K. // *ISIJ International.* 2013. V. 53. N 11. P. 1953.
- [123] Akioka K., Nakazawa T., Doi T., Arai M., Tsuji K. // *Powder Diffr.* 2014. V. 29. N 2. P. 151.
- [124] Menzel M., Schlifke A., Falk M., Janek J., Fröba M., Fittschen U.E.A. // *Spectrochim. Acta B.* 2013. V. 85. P. 62.

- [125] Baker A.M., Cai Y., Ziegelbauer J.M., Agyeman-Budu D., Woll A., Kongkanand A., Mukundan R., Borup R.L. // *ECS Trans.* 2019. V. 92. N 8. P. 107.
- [126] Tsuji K., Yonehara T., Nakano K. // *Anal. Sci.* 2008. V. 24. N 1. P. 99.
- [127] Perez R. D., Sanchez H. J., Perez C. A., Rubio M. // *Radiat. Phys. Chem.* 2010. V. 79. N 2. P. 195.
- [128] McCormick N., Velasquez V., Finney L., Vogt S., Kelleher S.L. // *PLoS ONE.* 2010. V. 5. P. e11078.
- [129] Rauwolf M., Turyanskaya A., Roschger A., Probst J., Simon R., Scharf O., Radtke M., Schoonjans T., Guilherme Buzanich A., Klaushofer K., Wobrauschek P., Hofstaetter J. G., Roschger P., Strelci C. // *J. Synchrotron Rad.* 2017. V. 24. N 1. P. 307.
- [130] Vincze L., Vekemans B., Brenker F.E., Falkenberg G., Rickers K., Somogyi A., Kersten M., Adams F. // *Anal. Chem.* 2004. V. 76. N 22. P. 6786.
- [131] Schmitz S., Müller A., Wilke M., Malzer W., Kanngieser B., Bousquet R., Berger A., Schefer S. // *Eur. J. Mineral.* 2009. V. 21. N 5. P. 927.
- [132] Jiang B., Zhu Y., Sun T., Liu Z., Li F., Sun X., Wang Y., Ding K. // *Spectrosc. Lett.* 2017. V. 50. N 10. P. 545.
- [133] Choudhury S., Swanston T., Varney T.L., Cooper D.M.L., George G.N., Pickering I.J., Grimes V., Bewer B., Coulthard I. // *Archaeometry.* 2016. V. 58. N S1. P. 207.
- [134] Choudhury S., Agyeman-Budu D.N., Woll A.R., Swanston T., Varney T.L., Cooper D.M.L., Hallin E., George G.N., Pickering I.J., Coulthard I. // *J. Anal. At. Spectrom.* 2017. V. 32. N 3. P. 527.
- [135] Hampai D., Liedl A., Cappuccio G., Capitolo E., Iannarelli M., Massucci M., Tucci S., Sardella R., Sciancalepore A., Polese C., Dabagov S.B. // *Nucl. Instrum. Methods Phys. Res. B.* 2017. V. 402. P. 274.
- [136] Nakano K., Nishi C., Otsuki K., Nishiwaki Y., Tsuji K. // *Anal. Chem.* 2011. V. 83. N 9. P. 3477.
- [137] Emoto S., Otsuki K., Nakano K., Tsuji K. // *Adv. X-Ray Anal.* 2013. V. 56. P. 217.
- [138] Sun X., Zhang X., Wang X., Wang Y., Li Y., Peng S., Shao S., Liu Z., Shang H., Sun T. // *X-Ray Spectrom.* 2020. V. 49. N 2. P. 267.
- [139] Fittschen U.E.A., Falkenberg G. // *Anal. Bioanal. Chem.* 2011. V. 400. N 6. P. 1743.
- [140] Schmitz S., Brenker F.E., Schoonjans T., Vekemans B., Silversmit G., Vincze L., Burghammer M., Riekel C. // *Geochim. Cosmochim. Acta* 2009. V. 73. N 6. P. 5483.
- [141] Mazel V., Reiche I., Busignies V., Walter P., Tchoreloff P. // *Talanta.* 2011. V. 85. N 1. P. 556.
- [142] Mihucz V.G., Silversmit G., Szalóki I., de Samber B., Schoonjans T., Tatár E., Vincze L., Virág I., Yao J., Záray G. // *Food Chem.* 2010. V. 121. N 1. P. 290.
- [143] Giacconi R., Rossi B. // *J. Geophys. Res.* 1960. V. 65. P. 773.
- [144] Wille E., Bavdaz M. // *Acta Astronautica.* 2015. V. 116. N 1. P. 50.
- [145] Saha T.T., McClelland R.S., Zhang W.W. // *Proc. SPIE.* 2014. V. 9144. P. 914418.
- [146] DeRoo C.T., Allured R., Cotroneo V., Hertz E., Marquez V., Reid P.B., Schwartz E.D., Vikhlinin A.A., Trolrier-McKinstry S., Walker J., Jackson T.N., Liu T.N., Tendulkar M. // *J. Astron. Telesc. Instrum. Syst.* 2018. V. 4. N 1. P. 019004.
- [147] Wallace K., Bavdaz M., Collon M., Beijersbergen M., Kraft S., Fairbend R., Séguy J., Blanquer P., Graue R., Kampf D. // *Proc. SPIE.* 2006. V. 10567. P. 105670U.
- [148] Beijersbergen M., Kraft S., Bavdaz M., Lumb D., Günther R., Collon M., Mieremet A., Fairbend R., Peacock A. // *Proc. SPIE.* 2004. V. 5539. P. 104.
- [149] Wille E., Wallace K., Bavdaz M., Collon M.J., Günther R., Ackermann M., Beijersbergen M.W., Riekerink M.O., Blom M., Lansdorp B., de Vreede L. // *Proc. SPIE.* 2017. V. 10565. P. 105652L.
- [150] Westergaard N.J., Ferreira D.D.M., Massahi S. // *Nucl. Instrum. Methods Phys. Res. A.* 2017. V. 873. N 21. P. 5.
- [151] Bavdaz M., Lumb D., Peacock A., Beijersbergen M., Kraft S. // *Proc. SPIE.* 2004. V. 5488. P. 829.
- [152] Chapman H.N., Nugent K.A., Wilkins S.W., Davis T.J. // *J. X-Ray Sci. Technol.* 1990. V. 2. N 2. P. 117.
- [153] Laprade B., Cochran R.C., Langevin F., Dykstra M.W. // *Proc SPIE.* 1997. V. 3173. P. 474.
- [154] Willingale R., Fraser G.W., Brunton A.N., Martin A.P. // *Exp. Astron.* 1998. V. 8. N 4. P. 281.
- [155] Beijersbergen M.W., Bavdaz M., Peacock A.J., Tomaselli E., Fraser G., Brunton A., Flyckt E., Krumrey M.K., Souvorov A. // *Proc. SPIE.* 1999. V. 3765. P. 452.
- [156] Collon M., Beijersbergen M., Wallace K., Bavdaz M., Fairbend R., Séguy J., Schyns E., Krumrey M., Freyberg M. // *Proc. SPIE.* 2007. V. 6688. P. 668812.
- [157] Wallace K., Collon M., Beijersbergen M., Oemrawsingh S., Bavdaz M., Schyns E. // *Proc. SPIE.* 2007. V. 6688. P. 66881C.
- [158] Price G.J., Brunton A.N., Beijersbergen M.W., Fraser G.W., Bavdaz M., Boutot J.P., Fairbend R., Flyckt S.O., Peacock A., Tomaselli E. // *Nucl. Instrum. Methods Phys. Res. A.* 2002. V. 490. N 1–2. P. 276.
- [159] Gotz D., Osborne J., Cordier B., Paul J., Evans P., Beardmore A., Martindale A., Willingale R., O'Brien P., Basa S., Rossin C., Godet O., Webb N., Greiner J., Nandra K., Meidinger N., Perinati E., Santangelo A., Mercier K., Gonzalez F. // *Proc. SPIE.* 2014. V. 9144. P. 914423.
- [160] Ezoë Y., Koshiishi M., Mita M., Mitsuda K., Hoshino A., Ishisaki Y., Yang Z., Takano T., Maeda R. // *Appl. Opt.* 2006. V. 45. N 35. P. 8932.
- [161] Ezoë Y., Koshiishi M., Mita M., Mitsuda K., Hoshino A., Ishisaki Y., Takano T., Maeda R. // *Nucl. Instrum. Methods Phys. Res. A.* 2007. V. 579. N 2. P. 817.
- [162] Ezoë Y., Mitsuishi I., Takagi U., Koshiishi M., Mitsuda K., Yamasaki N.Y., Ohashi T., Kato F., Sugiyama S., Riveros R.E., Yamaguchi H., Fujihira S., Kanamori Y., Morishita K., Nakajima K., Maeda R. // *Microsyst. Technol.* 2010. V. 16. N 8-9. P. 1633.
- [163] Ezoë Y., Miyoshi Y., Kasahara S., Kimura T., Ishikawa K., Fujimoto M., Mitsuda K., Sahara H., Isobe N., Nakajima H., Ohashi T., Nagata H., Funase R., Ueno M., Branduardi-Raymont G. // *J. Astron. Telesc. Instrum. Syst.* 2018. V. 4. N 4. P. 046001.
- [164] Mitsuishi I., Ezoë Y., Takagi U., Mita M., Riveros R., Yamaguchi H., Kato F., Sugiyama S., Fujiwara K., Morishita K., Nakajima K., Fujihira S., Kanamori Y., Yamasaki N., Mitsuda K., Maeda R. // *Proc. SPIE.* 2009. V. 7360. P. 736040.
- [165] Riveros R. E., Yamaguchi H., Mitsuishi I., Takagi U., Ezoë Y., Kato F., Sugiyama S., Yamasaki N., Mitsuda K. // *Appl. Optics.* 2010. V. 49. N 18. P. 3511.

- [166] Nakajima K., Fujiwara K., Pan W., Okuda H. // *Nat. Mater.* 2005. V. 4. N 1. P. 47.
- [167] Schmidt W.H.K. // *Nucl. Instr. Meth.* 1975. V. 127. P. 285.
- [168] Angel J.R.P. // *Astrophys. J.* 1979. V. 233. P. 364.
- [169] Chapman H.N., Nugent K.A., Wilkins S.W. // *Rev. Sci. Instr.* 1991. V. 62. N 6. P. 1542.
- [170] Kaaret P., Geissbühler P. // *Proc. SPIE.* 1991. V. 1546. P. 82.
- [171] Kaaret P., Geissbühler P., Chen A., Glavinias E. // *Appl. Opt.* 1992. V. 31. N 34. P. 7339.
- [172] Peele A.G., Nugent K.A., Rode A.V., Gabel K., Richardson M.C., Strack R., Siegmund W. // *Appl. Opt.* 1996. V. 35. N 22. P. 4420.
- [173] Su L., Li W., Wu M., Su Y., Guo C., Ruan N., Yang B., Yan F. // *Appl. Opt.* 2017. V. 56. N 22. P. 6267.
- [174] Tamagawa T., Uchiyama K., Otsubo R., Yuasa T., Zhou Y., Mihara T., Ezoe Y., Numazawa M., Ishi D., Fukushima A., Suzuki H., Uchino T., Sakuta S., Ishikawa K., Enoto T., Sakamoto T. // *J. Astron. Telesc. Instrum. Syst.* 2020. V. 6. N 2. P. 025003.
- [175] Wiza J.L. // *Nucl. Instr. Meth.* 1979. V. 162. P. 587.
- [176] Grubsky V., Gertsenshteyn M., Shoemaker K., Jansson T. // *Proc. SPIE.* 2007. V. 6688. P. 66880P.
- [177] Willingale R., Pearson J.F., Martindale A., Feldman C.H., Fairbend R., Schyns E., Petit S., Osborne J. P., O'Brien P. T. // *Proc. SPIE.* 2016. V. 9905. P. 99051Y.
- [178] Mutz J.-L., Bonnet O., Fairbend R., Schyns E., Séguy J. // *Proc SPIE.* 2007. V. 6479. P. 64790F.
- [179] Peng S., Wei F., Guo Y., Ye Y. // *Opt. Eng.* 2019. V. 58. N 9. P. 093101.
- [180] Svendsen S., Knudsen E.B., Blake S., Oosterbroek T., Jegers A.S., Ferreira D.D.M., Prod'homme T., Short B.t, Willingale R., O'Brien P. // *Proc. SPIE.* 2019. V. 11119. P. 111191R.
- [181] Peele A.G., Irving T.H.K., Nugent K.A., Mancini D.C., Christenson T.R., Petre R., Brumby S.P., Priedhorsky W.C. // *Rev. Sci. Instrum.* 2001. V. 72. N 3. P. 1843.
- [182] Peele A.G., Vora K.D., Shew B.-Y., Loechl B., Harvey E.C., Hayes J.P. // *Microsyst. Technol.* 2007. V. 13. N 5. P. 511.
- [183] Fraser G.W., Brunton A.N., Bannister N.P., Pearson J.F., Ward M., Stevenson T.J., Watson D.J., Warwick B., Whitehead S., O'Brien P., White N., Jahoda K., Black K., Hunter S.D., Deines-Jones P., Priedhorsky W.C., Brumby S.P., Borozdin K.N., Vestrand T., Fabian A.C., Nugent K.A., Peele A.G., Irving T.H.K., Price S., Eckersley S., Renouf I., Smith M., Parmar A.N., McHardy I.M., Uttley P., Lawrence A. // *Proc. SPIE.* 2002. V. 4497. P. 115.
- [184] Branduardi-Raymont G., Sembay S.F., Eastwood J.P., Sibeck D.G., Abbey A., Brown P., Carter J.A., Carr C.M., Forsyth C., Kataria D., Kemble S., Milan S.E., Owen C.J., Peacocke L., Read A.M., Coates A.J., Collier M.R., Cowley S.W.H., Fazakerley A.N., Fraser G.W., Jones G.H., Lallement R., Lester M., Porter F.S., Yeoman T.K. // *Exp. Astron.* 2012. V. 33. N 2. P. 403.
- [185] Collier M.R., Scott Porter F., Sibeck D.G., Carter J.A., Chiao M.P., Chornay D.J., Cravens T.E., Galeazzi M., Keller J.W., Koutroumpa D., Kujawski J., Kuntz K., Read A.M., Robertson I.P., Sembay S., Snowden S.L., Thomas N., Uprety Y., Walsh B.M. // *Rev. Sci. Instrum.* 2015. V. 86. N 7. P. 071301.
- [186] Walsh B.M., Collier M.R., Kuntz K.D., Porter F.S., Sibeck D.G., Snowden S.L., Carter J.A., Collado-Vega Y., Connor H.K., Cravens T.E., Read A.M., Sembay S., Thomas N.E. // *J. Geophys. Res. Space Physics.* 2016. V. 121. N 4. P. 3353.
- [187] Raab W., Branduardi-Raymont G., Wang C., Dai L., Donovan E., Enno G., Escoubet P., Holland A., Jing L., Kataria D., Li L., Read A., Rebuffat D., Romstedt J., Runciman C., Sembay S., Spanswick E., Sykes J., Thornhill J., Welders A., Zhang A., Zheng J. // *Proc. SPIE.* 2016. V. 9905. P. 990502.
- [188] Feldman C., Pearson J., Willingale R., Sykes J., Drumm P., Houghton P., Bicknell C., Osborne J., Martindale A., O'Brien P., Fairbend R., Schyns E., Petit S., Roudot R., Mercier K., Le Duigou J., Gotz D. // *Proc. SPIE.* 2017. V. 10399. P. 103991Q.
- [189] Amati L., O'Brien P., Götz D., Bozzo E., Tenzer C., Frontera F., Ghirlanda G., Labanti C., Osborne J.P., Stratta G., Tanvir N., Willingale R., Attina P., Campana R., Castro-Tirado A.J., Contini C., Fuschino F., Gomboc A., Hudec R., Orleanski P. // *Adv. Space Res.* 2018. V. 62. N 4. P. 191.
- [190] Korecki P., Sowa K.M., Jany B.R., Krok F. // *Phys. Rev. Lett.* 2016. V. 116. N 23. P. 233902.
- [191] Sowa K.M., Jany B.R., Korecki P. // *Optica.* 2018. V. 5. N 5. P. 577.
- [192] Nomoto K., Hata R., Doi K., Nawaki Y., Yajima D., Furuya R., Shinoda K., Tsuruoka K., Kodaka H. // *Proc. SPIE.* 2018. V. 10760. P. 107600A.
- [193] Doi K., Nomoto K., Nawaki Y., Uetsuki K., Hata R., Tsuruoka K., Kodaka H., Ito H., Harada Y., Asakawa Y. // *Proc. SPIE.* 2019. V. 11108. P. 11080V.
- [194] Gertsenshteyn M., Jansson T., Savant G. // *Proc. SPIE.* 2005. V. 5922. P. 59220N.
- [195] Ashcraft C. // *Creation.* 2010. V. 32. N 3. P. 21.